NASA/TM–20250006620

System-Level Single Event Effects Test Report - PIRT 1280MVCam InGaAs Infrared Camera

Landen D. Ryder

Jean-Marie Lauenstein

Michael J. Campola

October 2024

NASA STI Program Report Series

The NASA STI Program collects, organizes, provides for archiving, and disseminates NASA's STI. The NASA STI program provides access to the NTRS Registered and its public interface, the NASA Technical Reports Server, thus providing one of the largest collections of aeronautical and space science STI in the world. Results are published in both non-NASA channels and by NASA in the NASA STI Report Series, which includes the following report types:

- TECHNICAL PUBLICATION. Reports of completed research or a major significant phase of research that present the results of NASA Programs and include extensive data or theoretical analysis. Includes compilations of significant scientific and technical data and information deemed to be of continuing reference value. NASA counterpart of peer-reviewed formal professional papers but has less stringent limitations on manuscript length and extent of graphic presentations.

- TECHNICAL MEMORANDUM. Scientific and technical findings that are preliminary or of specialized interest, e.g., quick release reports, working papers, and bibliographies that contain minimal annotation. Does not contain extensive analysis.

- CONTRACTOR REPORT. Scientific and technical findings by NASA-sponsored contractors and grantees.

- CONFERENCE PUBLICATION. Collected papers from scientific and technical conferences, symposia, seminars, or other meetings sponsored or co-sponsored by NASA.

- SPECIAL PUBLICATION. Scientific, technical, or historical information from NASA programs, projects, and missions, often concerned with subjects having substantial public interest.

- TECHNICAL TRANSLATION. English-language translations of foreign scientific and technical material pertinent to NASA's mission.

Specialized services also include organizing and publishing research results, distributing specialized research announcements and feeds, providing information desk and personal search support, and enabling data exchange services.

For more information about the NASA STI program, see the following:

- Access the NASA STI program home page at http://www.sti.nasa.gov

- Help desk contact information:

https://www.sti.nasa.gov/sti-contact-form/
and select the "General" help request type.

NASA/TM–20250006620

System-Level Single Event Effects Test Report - PIRT 1280MVCam InGaAs Infrared Camera

Landen D. Ryder
Goddard Space Flight Center, Greenbelt, MD

Jean-Marie Lauenstein
Goddard Space Flight Center, Greenbelt, MD

Michael J. Campola
Goddard Space Flight Center, Greenbelt, MD

Test Date: 10/29/2024

National Aeronautics and
Space Administration

Goddard Space Flight Center
Greenbelt, MD 20771

October 2024

Acknowledgments

This work was sponsored by the NASA Electronic Parts and Packaging (NEPP) Program and supported by the Aerosol Radiometer for Global Observation of the Stratosphere (ARGOS) program.

Level of Review: This material has been technically reviewed by technical management.

Available from

NASA STI Program
Mail Stop 148
NASA's Langley Research Center
Hampton, VA 23681-2199

National Technical Information Service
5285 Port Royal Road
Springfield, VA 22161
703-605-6000

This report is available in electronic form at

https://nepp.nasa.gov/

I. Introduction

This irradiation test campaign was conducted to provide a "first pass screen" for persistent single event functional interrupts (SEFIs) and destructive single event effects in a commercial-off-the-shelf InGaAs camera system under consideration for space-based instrumentation. Testing was performed at NASA's Space Radiation Laboratory (NSRL) at Brookhaven National Laboratory (BNL) to ensure that heavy ions had sufficient energy to pass through the camera housing and multiple stacked printed circuit boards.

II. Device Under Test

Princeton Infrared Technologies' (PIRT) 1280MVCam is a shortwave infrared (SWIR) imager (1.7 µm cutoff wavelength) integrated with support electronics into an aluminum housing to provide an all-in-one imaging system. The system utilizes a backside illuminated, substrate-removed InGaAs focal plane array (FPA) with a 12 µm pixel pitch and 1280x1024 resolution. Presumably each pixel is indium bump-bonded to a Si CMOS read-out integrated circuit (ROIC) based on a capacitive transimpedance amplifier (CTIA) with a 14-bit analog-to-digital conversion. A single stage thermoelectric cooler (TEC) is included to stabilize the temperature of the FPA within a user defined temperature range.

To support image acquisition via the FPA, a wide array of support electronics is integrated into the camera housing on three stacked printed circuit boards populated on both sides with commercial electrical, electronic, electromechanical, and electrooptical (EEEE) parts with little-to-no existing radiation test data. The image processing and digital control functions are performed via a field programmatic gate array (FPGA) with an embedded ARM processor. Communication and data transfer from the system relies on universal asynchronous receiver-transceiver (UART) through the Camera Link standard. The system requires a dedicated power input of 12 V that is managed internally via regulators and DC/DC converters to provide the necessary voltage channels to power the FPA, TEC, and FPGA.

Figure 1. Picture of the 1280MVCam in a standard package. The camera that was evaluated during this test campaign had a custom aluminum enclosure.

Table I: Part Identification Information

Qty	Generic Part Number	Date Code	Package	REAG ID
1	1280MVCam	210019	Custom	24-016

III. Test Description

Interfacing with the camera system is accomplished via the Camera Link connection that is connected to a frame grabber installed into a local computer that is running PIRT's LabVIEW software. Utilizing this software, the camera system can be commanded to send a single or multiple image frames over the Camera Link connection for display and data capture. The camera system was configured to output continuous images during irradiation to screen for SEFI signatures in the captured images. Post run image processing via pixel histograms was performed following each irradiation using ImageJ software. An example image capture and image histogram is provided in Fig. 2.

In addition to image data, the Camera Link connection is utilized to set and monitor system configuration via a terminal connection facilitated by PIRT's LabVIEW software graphical user interface. For the purposes of the test, the serial connection was utilized prior to every run to modify the ADC resolution and TEC set point from base values set during camera initialization on power-up. For each run, a series of commands was sent via the serial connection to capture system configuration information pre- and post-irradiation to check for SEUs in configuration memory.

Since power management and conditioning is performed via internal electronics, current monitoring for data acquisition, over-current protection, and external power resets are performed via the single 12 V input port. The system-level current draw was monitored during irradiation to screen for irregular current behavior that is a signature of change in system configurations and SEFI states. An example current trace under nominal operation (reset, image capture, TEC enabled, and system configuration) is provided in Fig 3. Current limits were placed on the power supply to avoid high current states that would be indicative of a latch up in one of the constitutive integrated circuits (ICs).

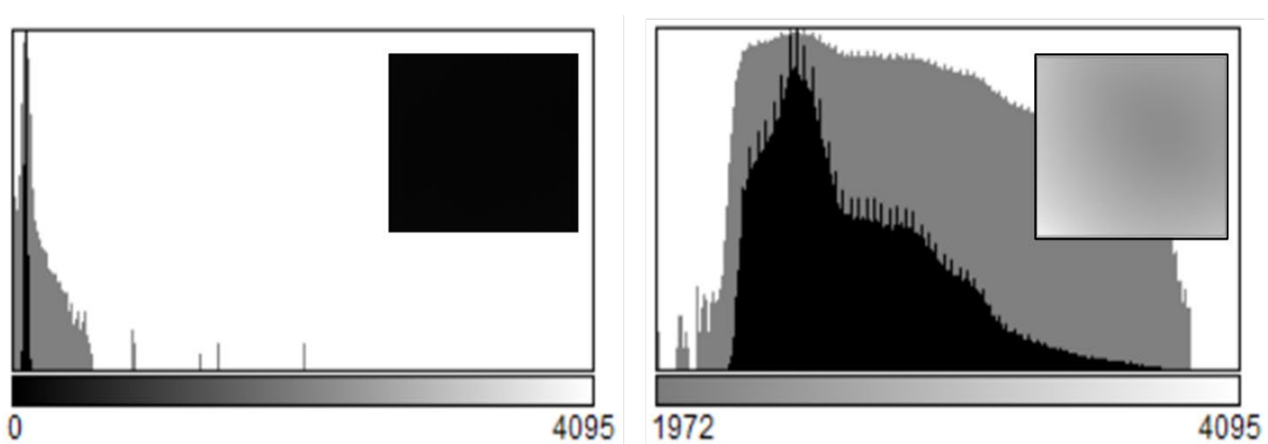

Figure 2. Two examples of pixel histograms with image frame inset in the right corner. Gray histogram bins are on log scale and black histogram bins are on a linear scale.

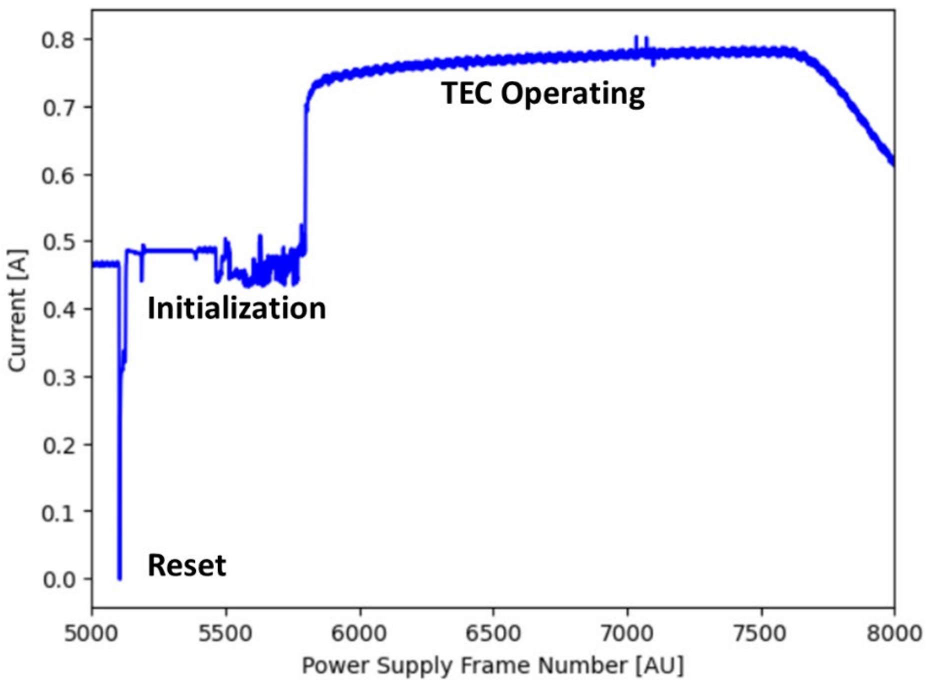

Figure 3. Example current trace for a reset of the camera and enabling of TEC.

IV. Test Setup

The camera system was positioned in the beam with the image sensing element placed facing the beam port and held via a clamp holding the aluminum housing (Fig. 4). A black light blocking cloth cover was placed over the image sensing element to facilitate dark images during testing. The 12 V input port is connected to the nearby power supply via a modified version of the wall adapter. The Camera Link port is connected via short cabling to a frame grabber installed in a nearby computer that runs the PIRT software to control the camera system to view and save image data. The power supply and computer with frame grabber are remotely accessed via 100 ft ethernet cable runs and signal extenders. Table II lists the specific equipment for this test. A representative block diagram of the test setup is provided in Fig. 5.

Prior to each irradiation run, the camera system is power cycled via toggling of the power supply channel to clear any latent errors and reinitialize the camera system to a known configuration state. Additional commands are then sent to the camera system to modify the TEC setting and the resolution of the ADC to better represent the intended mission application and then report out the pre-irradiation configuration values. During irradiation the camera system is set to continuous image capture and the irradiation can be stopped early if the camera system loses required functionality or a target fluence is reached. Following each run the configuration values are reported out to check against pre-irradiation values. See Appendix A for the initial configuration commands and the query of configuration values used as a health check.

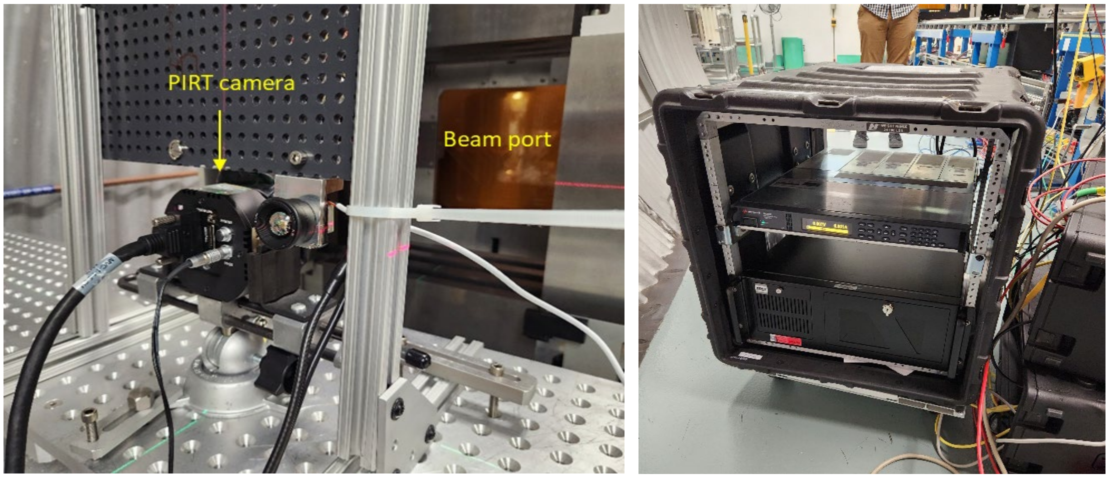

Figure 4. Left: Camera system positioned in beam line. Laser beams are part of NSRL alignment system. Right: Power supply and computer (with frame grabber) in cave adjacent to beam port.

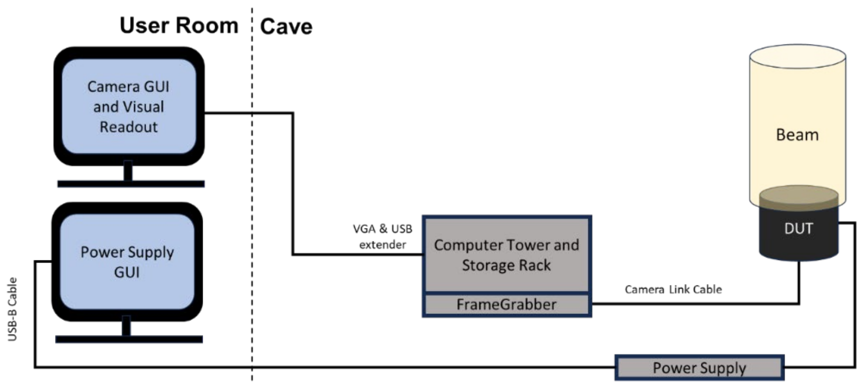

Figure 5. Block diagram of test setup used.

Table II: Equipment List

Equipment	Functionality
BitFlow Frame-Grabber	Communication with the camera system
ADEK Model 586-02B Computer	Camera interface and data storage
Keysight N6702C power supply	Powers the camera system and measure current draw
Dell PRECISION 7730 Lab Computer	Remote control of the power supply

V. Test Facility and Irradiation Conditions

Facility: NASA Space Radiation Laboratory at Brookhaven National Laboratory.
Average Flux: 3.1 x 10^2 ions/cm^2/s to 6.3 x 10^3 ions/cm^2/s.
Fluence: All tests were to be run to 1 x 10^7 ions/cm^2 .
Ion Species: Table III summarizes the facility-provided beam energy and surface-incident beam properties that were planned for use. As the ions will be passing through layers of aluminum housing and stacked PCBs (see Fig. 7), Table IV provides estimates of linear energy transfer (LET) at the front and back of each PCB as calculated via NSRL StackUp Calculator based on Ziegler's SRIM code.
Temperature: Ambient room temperature, with camera TEC maintaining the FPA at 15 °C.

Table III: Ion Information

Ion	Surface Energy [MeV/nucleon]	Surface LET [MeV·cm^2/mg]	Range in Silicon [mm]	Angle of Incidence [Degrees]
Fe	480	1.5	49.8	0
Fe	285	1.9	21.6	0
Ag	575	4.6	27.0	0
Ag	460	5.0	27.0	0
Tb	446	9.3	21.4	0
Tb	370	10.1	5.6	0

Table IV: LET Estimates at Each Side of the 3 PCBs

Board Location	Fe		Ag		Tb	
	480 MeV/u	285 MeV/u	575 MeV/u	460 MeV/u	446 MeV/u	370 MeV/u
Top of PCB 1	1.6	2.8	5.2	6.3	12.6	18.9
Bottom of PCB 1	1.7	2.9	5.3	6.4	13.3	22.9
Top of PCB 2	1.7	2.9	5.3	6.4	13.4	23.5
Bottom of PCB 2	1.7	3.1	5.4	6.6	14.2	37.2
Top of PCB 3	1.7	3.2	5.4	6.7	14.3	40.8
Bottom of PCB 3	1.7	3.4	5.5	6.9	15.4	-

VI. Results

Overall, persistent SEFI behavior was observed with particle species and energies corresponding to the lowest LET considered in this test campaign (~1.6 MeV·cm^2/mg). These SEFIs primarily presented as a loss in communication with the camera that required a power reset to clear. After a couple of runs, the system configuration was changed from continuous image acquisition to single frame acquisition to slightly extend the length of the run before the communication with the camera was lost. Following run seven, the camera system was found to be in an unrecoverable state that could not be resolved with power resets. The system was checked again approximately 48 hours post-irradiation and it was still in an inoperable state. A summary of irradiation run parameters and associated error signatures is provided in Table V and VI respectively.

A core requirement of SEE testing is that the system remain in a nominal operating state during irradiation to ensure that erroneous states do not mask the onset of additional error states or destructive SEEs. For this test campaign, SEFI states occurred so quickly after the start of a run that it was not feasible to collect accurate fluence-to-SEFI values required to create cross-sections required for error rate calculations. In addition, SEL susceptibility could not be assessed and remains a potential vulnerability. The following section extracts qualitative observations that may aid in the identification of the components creating the system errors.

Table V: Run Information

Run	Ion Species [MeV/nucleon]	Image Capture	Run Fluence [ions/cm^2]	Average Flux [ions/cm^2/s]
1	Fe – 480	Continuous	9.49E+04	-
2		Continuous	2.26E+04	8.81E+02
3		Single Frame	5.87E+03	3.67E+02
4		Single Frame	2.26E+03	1.77E+02
5		Single Frame	6.71E+04	2.38E+02
6		Single Frame	3.94E+05	6.48E+03
7		Single Frame	5.99E+06	3.39E+03

Table VI: Run Observations

Run	Failure Notes
1	Loss of communication with camera; no image frames or response to console commands.
2	Drop in current and loss of communication with camera; no image frames or console commands
3	Single frame acquisition; drop in current; loss of console commands but could still capture indiv. frames until late in run
4	Similar to run 3
5	Current increase and loss of communication; several frame acquisitions until streaking observed
6	Seemingly self-power cycled; lost communication with camera and image capture
7	Camera communication lost quickly; system allowed to run during irradiation while monitoring the LED on camera enclosure; LED blinking rapidly in error mode, then LED ceased and subsequent power resets could not bring camera back.

During irradiation, ions passing through the FPA will deposit energy in the detector material and be captured in the image frames similar to the infrared photons that the system is designed for. This single-event transient pixel behavior is typically not subject to scrutiny as ion fluxes during missions are much lower than in a ground-based heavy ion tests and are considered to impact single frames of image data. Figure 8 provides a sub-region of the FPA to demonstrate the distribution of pixel cluster sizes that the ionizing particles can create when striking at normal incidence; in some applications SEE data can be used to discriminate between the intended photon measurements and incident ionizing particles. For system-level radiation testing, histograms can be used to identify more rapidly SEFI signatures in the image capture and discriminate between ions being captured in individual frames (Fig. 8) and persistent errors (Fig. 9). The persistent behavior identified in Fig. 9 strongly resembles image data before the resolution of the ADC is modified to 12 bits and is therefore indicative of either an upset in the configuration logic or a system power reset induced return to the 14-bit resolution configuration that is automatically set at start up.

Because every run was terminated due to loss of communication failure with the camera system, it was not possible to check and record system configuration via console commands for post-irradiation comparisons prior to a system reset and reconfiguration. There does not appear to be anomalous changes in configuration states following a system reset, suggesting that communication loss is not occurring downstream of the boot flash loading initial system configuration to the FPGA/processor.

Run seven can be decomposed into three distinct time intervals: errors are cleared when observed, errors were allowed to persist, and the system became unrecoverable (Fig. 10). The current draw of the system during this final run is useful for examining potential failure modes and signatures. As the camera system is left in the error state, it is notable that 1) the elevated current associated with enabling the TEC following each reset is no longer observed, 2) the average currents remain roughly the same, and 3) the brief drops in current associated with power cycling are still observed with no manual resets. These observations suggest that in addition to errors in communication components and configuration memory, it appears that there are SEE-induced power resets that could originate in control logic, power management ICs, or supervisory circuitry.

As the camera system became unrecoverable, the average current dropped approximately 30% but maintained relatively consistent current draw. This behavior suggests that there are still functioning ICs within the system and it may be possible to identify suspect parts by reviewing the per component power budgets. Given the size of the current reduction, power management ICs, FPGA/processor, and various memories would be reasonable candidates for further investigation. It should be noted that no high current states were observed during this test campaign and it therefore unlikely that the system was rendered inoperable due to destructive SEEs at this test LET.

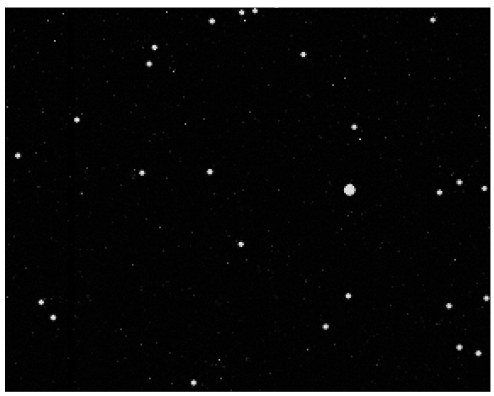

Figure 7. A subregion of an image captured during a beam spill. Note that an individual ion's generated charge may be collected within an individual pixel or across clusters of pixels.

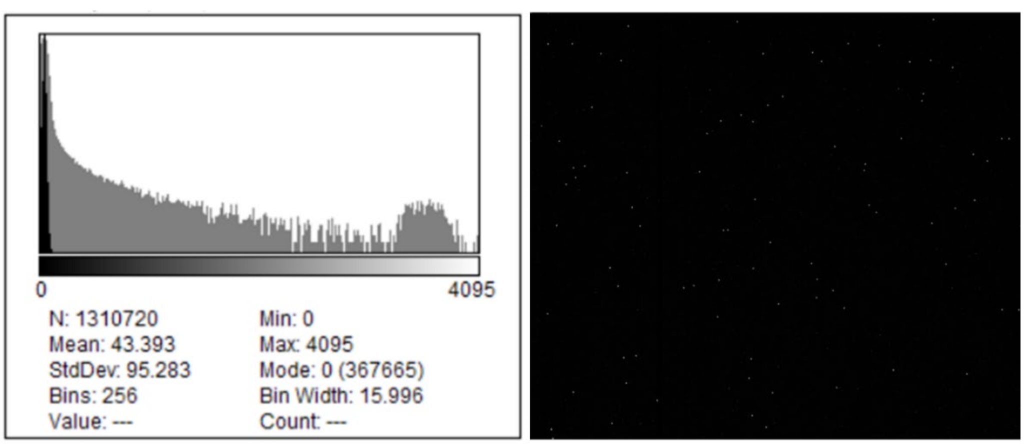

Figure 8. Image frame that has captured ions passing through the FPA pixels.

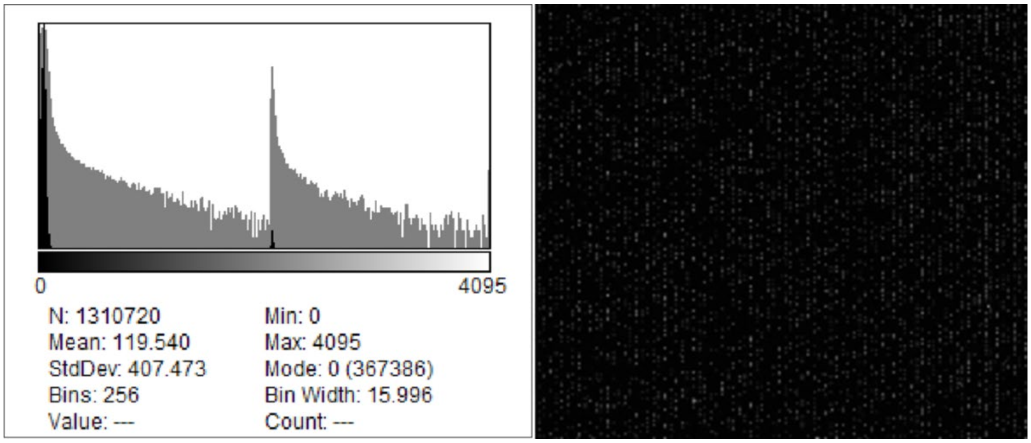

Figure 9. Subregion of image frame showing "streaking" that likely corresponds to an SEE that impacts the bit resolution of the ADC. Histogram is of entire image.

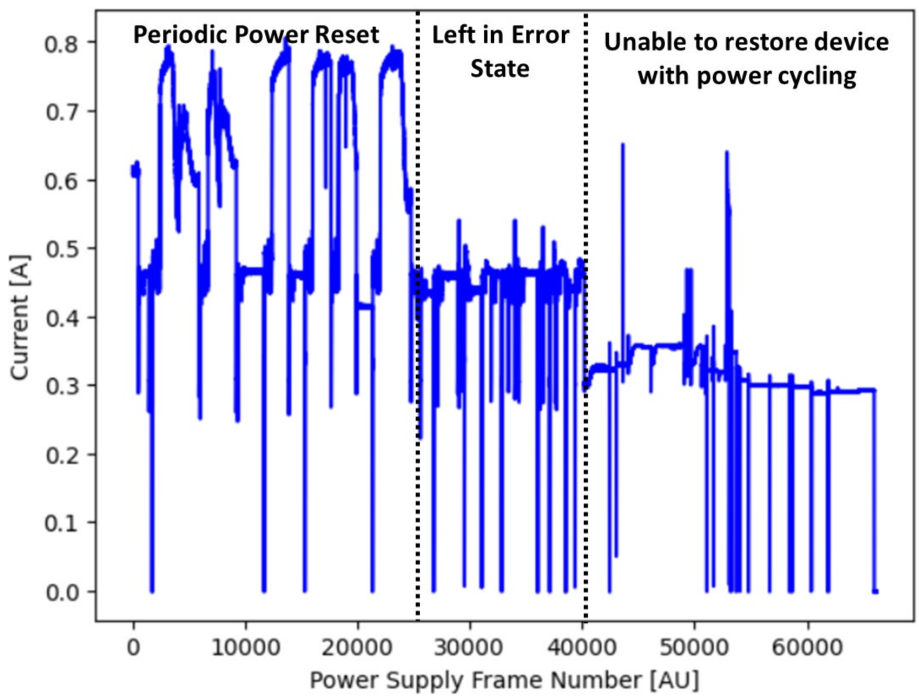

Figure 10. Current trace behavior capturing the "system failure" that has been unrecoverable. Note that the average current draw decreases after the failure.

VII. Summary

A system-level SEE test campaign was carried out on a COTS InGaAs camera system utilizing high energy, long range ions available at NSRL to provide a "first pass screen" for persistent SEFI signatures and destructive SEEs that would significantly impact system reliability and availability in flight projects. One unit was available for testing and particle species and energy were selected to gradually increase to achieve maximize data collection and search for threshold LET for various system behaviors. **Persistent**

communication errors were observed at the lowest LET (1.6 MeV·cm^2/mg) with minimal test fluences and eventually led to unrecoverable system failure. This dominant error behavior prevented the investigation of other error signatures; thus, these test results do not preclude other failure modes at this LET. No conclusions can be drawn regarding susceptibility to destructive SEE.